



**HAL**  
open science

## Evidence from numerical modelling for 3D spreading of [001] screw dislocations in Mg<sub>2</sub>SiO<sub>4</sub> forsterite

Ph. Carrez, Andrew M Walker, Arnaud Metsue, P Cordier

► **To cite this version:**

Ph. Carrez, Andrew M Walker, Arnaud Metsue, P Cordier. Evidence from numerical modelling for 3D spreading of [001] screw dislocations in Mg<sub>2</sub>SiO<sub>4</sub> forsterite. *Philosophical Magazine*, 2008, 88 (16), pp.2477-2485. 10.1080/14786430802363804 . hal-00513947

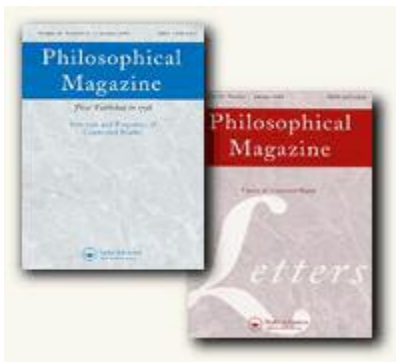
**HAL Id: hal-00513947**

**<https://hal.science/hal-00513947>**

Submitted on 1 Sep 2010

**HAL** is a multi-disciplinary open access archive for the deposit and dissemination of scientific research documents, whether they are published or not. The documents may come from teaching and research institutions in France or abroad, or from public or private research centers.

L'archive ouverte pluridisciplinaire **HAL**, est destinée au dépôt et à la diffusion de documents scientifiques de niveau recherche, publiés ou non, émanant des établissements d'enseignement et de recherche français ou étrangers, des laboratoires publics ou privés.



**Evidence from numerical modelling for 3D spreading of [001] screw dislocations in Mg<sub>2</sub>SiO<sub>4</sub> forsterite**

|                               |   |
|-------------------------------|---|
| Journal:                      | <i>Philosophical Magazine &amp; Philosophical Magazine Letters</i>  |
| Manuscript ID:                | TPHM-08-Jun-0229.R1   |
| Journal Selection:            | Philosophical Magazine  |
| Date Submitted by the Author: | 21-Jul-2008   |
| Complete List of Authors:     | Carrez, Ph.; Université des Sciences et Technologies de Lille, Laboratoire de Structure et Propriétés de l'Etat Solide<br>Walker, Andrew; University of Cambridge, Department of Earth Sciences<br>Metsue, Arnaud; Université des Sciences et Technologies de Lille, Laboratoire de Structure et Propriétés de l'Etat Solide<br>Cordier, P; Université des Sciences et Technologies de Lille, Laboratoire de Structure et Propriétés de l'Etat Solide |
| Keywords:                     | computer modelling, defect structures, dislocations, minerals   |
| Keywords (user supplied):     | computer modelling, defect structures, dislocations   |
|                               |   |



1  
2  
3 **Evidence from numerical modelling for 3D spreading of [001] screw dislocations in**  
4 **Mg<sub>2</sub>SiO<sub>4</sub> forsterite**  
5  
6  
7  
8  
9

10 Ph. Carrez<sup>a</sup>, A.M. Walker<sup>b</sup>, A. Metsue<sup>a</sup> and P. Cordier<sup>a</sup>  
11

12  
13  
14 *<sup>a</sup>Laboratoire de Structure et Propriétés de l'Etat Solide, UMR CNRS 8008, Université des*  
15 *Sciences et Technologies de Lille, 59655 Villeneuve d'Ascq Cedex, France*  
16

17 *<sup>b</sup>Department of Earth Sciences, University of Cambridge, Downing Street, Cambridge, CB2 3EQ,*  
18 *UK*  
19

20  
21  
22 *Second version, revised July, 20<sup>th</sup>, 2008*  
23  
24  
25  
26  
27  
28

29 Corresponding author:  
30

31 Patrick Cordier  
32

33 Laboratoire de Structure et Propriétés de l'Etat Solide - UMR CNRS 8008  
34

35 Université des Sciences et Technologies de Lille - Bat C6  
36

37 59655 Villeneuve d'Ascq Cedex - FRANCE  
38

39 Phone: (33) 03 20 43 43 41  
40

41 Fax: (33) 03 20 43 65 91  
42

43 E-mail: [Patrick.Cordier@univ-lille1.fr](mailto:Patrick.Cordier@univ-lille1.fr)  
44  
45  
46

47 Manuscript prepared with Word X on Macintosh  
48  
49  
50  
51  
52  
53  
54  
55  
56  
57  
58  
59  
60

1  
2  
3  
4  
5  
6  
7  
8  
9  
10  
11  
12  
13  
14  
15  
16  
17  
18  
19  
20  
21  
22  
23  
24  
25  
26  
27  
28  
29  
30  
31  
32  
33  
34  
35  
36  
37  
38  
39  
40  
41  
42  
43  
44  
45  
46  
47  
48  
49  
50  
51  
52  
53  
54  
55  
56  
57  
58  
59  
60

For Peer Review Only

1  
2  
3  
4  
5  
6  
7  
8  
9  
10  
11  
12  
13  
14  
15  
16  
17  
18  
19  
20  
21  
22  
23  
24  
25  
26  
27  
28  
29  
30  
31  
32  
33  
34  
35  
36  
37  
38  
39  
40  
41  
42  
43  
44  
45  
46  
47  
48  
49  
50  
51  
52  
53  
54  
55  
56  
57  
58  
59  
60

**Abstract:** Computer simulations have previously been used to derive the atomic scale properties of the cores of screw dislocations in  $\text{Mg}_2\text{SiO}_4$  forsterite by direct calculation using parameterised potentials and via the Peierls-Nabarro model using density functional theory. We show that, for the [001] screw dislocation, the parameterised potentials reproduce key features of generalised stacking fault energies when compared to the density functional theory results, but that the predicted structure of the dislocation core differs between direct simulation and the Peierls-Nabarro model. The [001] screw dislocation is shown to exhibit a low-energy non-planar core. It is suggested that for this dislocation to move its core may need to change structure and form a high-energy planar structure similar to that derived from the Peierls-Nabarro model. This could lead to dislocation motion via an unlocking-locking mechanism and explain the common experimental observation of long straight screw dislocation segments in deformed olivine.

**Keywords:** dislocation core, forsterite, numerical modelling, screw dislocations

## 1. Introduction

As the dominant constituent of the Earth's upper mantle, the rheology of  $(\text{Mg,Fe})_2\text{SiO}_4$  olivine plays a controlling role in solid-state mantle convection and its surface expression, plate tectonics. Numerous experimental studies have been undertaken to identify active slip systems in deformed olivine and the magnesium end-member, forsterite [1-3]. In olivine, the Burgers vectors correspond to the shortest lattice repeats of the orthorhombic (space group *Pbnm*) crystal structure, [100] and [001]. At ambient pressure, under conditions of low-temperature and high-stress, [001] dislocations gliding on (100), {110} and (010) are usually reported whereas [100] dislocations gliding on (010), (001), {031}, {021} and {011} dominate at high temperature [4]. No other slip systems are observed despite the fact that, according to the von Mises criterion [5], there are not enough active slip systems to permit polycrystalline deformation. Recent studies have shown that [001] glide is enhanced when pressure increases [6-10] or when trace amounts of water are incorporated into the olivine crystal structure [11, 12].

In a recent study [8] Durinck et al. have derived dislocation core structures based on the Peierls-Nabarro (PN) model. The tendency of [001] screw dislocations to spread into (100) and {110} glide planes led Durinck et al. [8] to speculate that [001] screw dislocations in olivine may exhibit a non-planar core, similar to that found in body centred cubic (bcc) metals (e.g. [13-15]). This hypothesis is supported by microstructural observations which always show that [001] glide is dominated by long straight screw dislocations (for instance [16, 2, 6]), implying that these dislocations experience large lattice friction stresses.

In the following, we want to clarify this assumption using results of full atomistic calculations of the [001] screw dislocation in forsterite. We compare the core structure of the [001] screw dislocation in forsterite calculated via direct atomistic simulation with that predicted by the PN model. For the direct atomistic simulations we reuse the results of calculations previously described by Walker et al. [17,18]. For consistency we calculate the generalised stacking fault (GSF) energies using the same potential model as that used for the direct simulations before applying the PN model to extract the core structure. The GSF calculations closely follow the methodology used by Durinck et al. [7, 8], who utilised density functional theory (DFT). This provides the opportunity to compare the GSF results of the potential model with those of DFT, allowing us to assess the ability of the potential model to cope with non-elastic deformation found at the core of dislocations.

## 2. Methodology

1  
2  
3 As recently reviewed by Schoeck [19, 20] and Woodward [21], the arrangement of atoms  
4 around a dislocation line can be obtained in two ways, either directly, using atomistic  
5 calculations, or from the Peierls-Nabarro model. Because of the computationally demanding  
6 need to include a large number of atoms, usually too many for *ab initio* methods, direct  
7 calculations are generally limited by the accuracy of a chosen interatomic potential model.  
8 This can be an important limitation [20], but fully *ab initio* simulations of dislocation cores in  
9 some simple materials are now becoming possible [22]. On the other hand, this approach  
10 requires few assumptions: in the simplest case the system must be periodic along the  
11 dislocation line and some approximate initial dislocation geometry must be used. The  
12 assumptions of the PN model are more severe. When one-dimensional GSF energies are used  
13 as input only pure edge or pure screw dislocations can be considered and spreading of the  
14 core is limited to the chosen glide plane [19]. However, the PN model can yield results in  
15 close agreement with direct atomistic calculations, even when the core structure is complex  
16 and the dislocation is dissociated, as is the case of NiAl [23, 24].  
17  
18  
19  
20  
21  
22  
23  
24  
25  
26  
27  
28  
29

### 30 **2.1. Direct atomistic simulation**

31 The direct atomistic simulations are described in detail elsewhere [17, 18], but key  
32 features of the methodology will be outlined here. The simulations were performed using a  
33 simulation cell that is periodic along the dislocation line and exhibits no periodicity in the two  
34 perpendicular directions. Strain associated with the dislocation was assumed to be well  
35 represented by anisotropic linear elasticity far from the core but this breaks down when the  
36 strain becomes large close to the core. In order to handle the non-linear effects and the atomic  
37 scale reconstruction of the core an atomistic model was used and this was embedded in the  
38 long-ranged elastic representation of the dislocated crystal. Although the elastic region can be  
39 allowed to respond to forces generated by the dislocation core (e.g. [21]) in these calculations  
40 the atoms around the rim of the simulation cell were held fixed at the location predicted by  
41 linear elasticity. The location of these atoms was therefore determined from only the  
42 dislocation's Burgers vector and elastic constants appropriate to the atomic model.  
43  
44  
45  
46  
47  
48  
49  
50  
51  
52

53 For the model of forsterite, an interatomic potential model with formal charges, fitted  
54 to the structure and some properties of quartz and binary oxides, was selected [25-27]. This  
55 model has been extensively used for studies of the thermodynamic and structural properties of  
56 perfect forsterite [28-30] as well as studies of surfaces [31-33] and point defects [34-37].  
57 Parameters of the model are given in Table 1. The use of a potential model with a long-ranged  
58 Coulomb component implies the need for special treatment of this part of the energy  
59  
60

1  
2  
3 calculation [17] and for care in building the simulation cell to avoid the creation of a charged  
4 simulation cell, or a cell with a large electrostatic dipole [18]. For the case of the [001] screw  
5 dislocation in forsterite this was achieved by using the Coulomb summation of Saunders et al.  
6 [38] and by building the simulation cell out of charge neutral units. The simulation cell has a  
7 radius of 75 Å and atoms in the outermost 25 Å rim were held fixed at the location given by  
8 linear elasticity. The model contained 15044 particles made up of 2658 magnesium atoms,  
9 1330 silicon atoms, 5528 oxygen cores and 5528 oxygen shells. The initial location of all the  
10 atoms were determined from linear elasticity and the inner atoms are moved to minimise the  
11 total energy using the GULP code [39].

## 2.2 Simulation via the Peierls-Nabarro model

22 The alternative method used to arrive at a geometry of the dislocation core involves  
23 solving the Peierls-Nabarro equation, which relates a continuous distribution of shear in the  
24 glide plane,  $S(x)$ , to a continuous distribution of infinitesimal dislocations with density  $\rho(x)$   
25 and a restoring force,  $F(S(x))$ :

$$\frac{K}{2\pi} \int_{-\infty}^{+\infty} \frac{1}{x-x'} \left[ \frac{dS(x')}{dx'} \right] dx' = \frac{K}{2\pi} \int_{-\infty}^{+\infty} \frac{\rho(x')}{x-x'} dx' = F(S(x)) \quad (1)$$

33 where  $K$  is the energy coefficient and  $x$  and  $x'$  are displacements in the glide plane. For any  
34 amount of shear the restoring force can be calculated from a set of atomistic models  
35 containing generalised stacking faults with different displacements. The restoring force is the  
36 gradient of the GSF energy with respect to displacement and full details of the solution are  
37 given in [8], which follows the methodology of Joos et al. [40]. GSF calculations were  
38 performed with the same potential model and computer code as was used for the direct  
39 modelling of the core. The geometry of the supercells used for these GSF calculations were  
40 chosen to be the same as those used for the DFT based GSF calculations [7] and identical  
41 relaxation conditions have been used (i.e. atoms were only allowed to move in a direction  
42 perpendicular to the stacking fault during the calculation). Using the same simulation cell as  
43 the previous DFT calculations allows the use of the DFT results as a reference: it is possible  
44 to directly compare the DFT and parameterised potential GSF calculations and understand the  
45 limitations of the potential model with respect to dislocation modelling.

56 Solving the PN equation provides the shear profile,  $S$ , and the distribution of Burgers  
57 vector density,  $\rho$ , across the dislocation core. In order to display the atomic arrangement in the  
58 dislocation core, we follow the approach for screw dislocations described by Eshelby [41] and  
59 reproduced in [42]. Thus, we start from a perfect crystal structure split into two semi-infinite  
60

1  
2  
3 half crystals with a disregistry of  $b/2$  for symmetry reasons. The atom positions in the (001)  
4 plane (normal to the dislocation line) are given as  $(x,y)$ . The PN dislocation is then introduced  
5 by attributing to all atoms a displacement,  $u$ , along the dislocation (parallel to the  $z$   
6 coordinates axis) calculated from the disregistry function  $S(x)$ . Finally, the core structure is  
7 given by introducing the elastic displacement field  $u_z(x,y)$ . For a [001] screw dislocation  
8 calculated in this study with anisotropic elasticity the displacement field is found from:  
9

$$10 \quad u_z(x,y) = \frac{1}{2\pi} \int_{-\infty}^{+\infty} \rho(x') \arctan\left(\sqrt{\frac{S_{44}}{S_{55}}} \frac{y}{x-x'}\right) dx' \quad (2)$$

11 where  $S_{44}$  and  $S_{55}$  are elements of the reduced elastic compliance matrix [43, 44].  
12  
13

### 14 **2.3. Geometrical analysis of the core structure of the [001] screw dislocation**

15 Although both methods of simulating the dislocation core reveal a detailed atomic  
16 structure, any comparison between the two is difficult. This is mostly because the  
17 displacements are predominantly parallel to the dislocation line and at first glance, looking  
18 along the line, it is hard even to differentiate between the dislocated and perfect crystal. A  
19 powerful method of analysing the core structure of a screw dislocation is to superimpose a  
20 differential displacement map on top of the atomic structure of the core. In particular, the  
21 difference in total displacement of two adjacent atoms along the dislocation line can be  
22 plotted as an arrow between the two atoms. The arrow length is proportional to the difference  
23 in displacement. This is known as the Vitek representation [45]. In this representation a screw  
24 dislocation in an isotropic elastic body would be represented by a circle of arrows of equal  
25 length around the core, with the length decreasing logarithmically with distance from the  
26 core. For  $\langle 111 \rangle$  screw dislocations in bcc metals three equivalent directions are clearly seen,  
27 representing the three-fold spreading of the core in  $\{110\}$  planes.  
28  
29

30 For forsterite, it is useful to only represent the differential displacement for the oxygen  
31 sublattice. Indeed, the oxygen sublattice of forsterite can be viewed as a slightly distorted  
32 hexagonal close packed (HPC) lattice and this leads to the maximum symmetry properties.  
33  
34  
35  
36  
37  
38  
39  
40  
41  
42  
43  
44  
45  
46  
47

## 48 **3. Results**

49 Results of the GSF calculations for the three slip systems are presented in Figure 1 and  
50 key parameters of the dislocation calculated from the PN model are presented in Table 2; in  
51 both cases the previous DFT results are compared with results from the potential model. The  
52  
53  
54  
55  
56  
57  
58  
59  
60

1  
2  
3 shapes of the GSF curves are clearly similar for the parameterised potentials and first  
4 principles calculations. In particular, we found a single peak in the GSF curve for [001](010),  
5 whereas [001](100) and [001]{110} are characterized by a camel-hump double peak shape.  
6 Quantitatively, energies differ between the two methods, especially for the (100) and {110}  
7 planes, with the maxima being larger for the potential model than for DFT. This excess in  
8 barrier height is likely to be due to the use of a potential model utilising formal charges, a  
9 similar effect was observed in a study of oxygen diffusion using the same potential model  
10 [46]. However, the ratio between the stacking fault energy (SFE, corresponding to the  
11 minimum exhibited at half shear) and the maximum of the GSF curves ( $\gamma^{\max}$ ) are more  
12 consistent and only differ for the (100) plane (Table 2). In agreement with [7], the SFE in the  
13 (100) and {110} planes are found to be very similar with a value of  $42 \text{ meV}/\text{\AA}^2$ . Finally, for  
14 the (010) plane for which the two types of calculations lead to similar GSF profiles, solution  
15 of the PN equation gives comparable extension of the screw dislocation core. For the potential  
16 model we find a dislocation core half-width of  $1.4 \text{ \AA}$ , close to the value of  $1.9 \text{ \AA}$  found by  
17 Durinck et al. [7].

18  
19  
20  
21  
22  
23  
24  
25  
26  
27  
28  
29  
30  
31  
32  
33  
34  
35  
36  
37  
38  
39  
40  
41  
42  
43  
44  
45  
46  
47  
48  
49  
50  
51  
52  
53  
54  
55  
56  
57  
58  
59  
60  
The geometry of the core of the [001] screw dislocation as predicted by direct  
calculation is presented in Figure 2. The  $\text{SiO}_4$  tetrahedra are preserved in the dislocation core.  
Few atomic positions differ from those in the perfect crystal since the dislocation line is  
viewed end-on. This emphasises the fact that atomic relaxation in the core are mostly parallel  
to the Burgers vector. To visualize the dislocation core geometry, the differential  
displacement of the oxygen sublattice is superimposed on the core structure in Figure 2. This  
clearly shows that the core is spread in several planes. This is dramatically different to the  
displacement predicted by the Peierls dislocation, which, as expected and shown in Figure 3,  
is confined within a single plane.

#### 4. Discussion

Whatever model is chosen, Figures 2 and 3 clearly show that the maximum relative  
displacements occur between atoms that do not belong to the same tetrahedra. This confirms  
that Si-O bonds are stiff and the tetrahedra act like rigid units. The total dislocation density is  
spread in such a way that the  $\text{SiO}_4$  tetrahedra are not deformed. The Peierls dislocation shown  
in Figure 3 has been constructed assuming a planar core. Indeed, the arrows are observed  
within the (010) layer located between two layers of tetrahedra. Compared to Figure 3, the  
dislocation shown in Figure 2 clearly deviates from a planar core since arrows are found in  
several layers. A large part of the dislocation density profile is located at the centre, between

1  
2  
3 the tetrahedra. A significant part of shear is spread out in two (010) planes. As a result, the  
4 [001] dislocation clearly exhibits a 3D core structure as anticipated by Durinck et al. [8]. The  
5 strong tendency of the shear distribution to be located in two (010) planes is very similar to  
6 the so-called zonal dissociation proposed for  $\langle a \rangle$  dislocations in quartz [47].  
7  
8  
9

10 We now have to ask what is physical relevance of these two models for the dislocation  
11 core structure? To answer this question, one must remember how they have been constructed.  
12 The Peierls model imposes a planar core. Hence, this dislocation is, by construction, the most  
13 able to glide in a given plane. No constraint is put on its energy. On the contrary, the direct  
14 model derives from an energy minimisation process. This dislocation is likely to be the most  
15 “stable” (lowest energy configuration), but not necessarily the most easy to glide. Indeed, we  
16 calculated the energy stored within the inner 10 Å of both models embedded within a 30 Å  
17 representation of the extended dislocated crystal while taking care to include the same atoms  
18 in each setup. This calculation showed that the PN core is up to 2.7 eV/Å higher in energy  
19 than the fully relaxed configuration (this is an upper bound on the energy difference as the  
20 location of the oxygen shells in the PN model can not be determined and the oxygen is thus  
21 not polarized).  
22  
23  
24  
25  
26  
27  
28  
29  
30  
31

32 We now discuss the implications of those two possible core configurations on  
33 dislocation mobility. Vitek suggested that the kink-pair mechanism in bcc metals corresponds  
34 to the transformation of a non-planar core into a planar core in the slip plane [48]. At rest,  
35 [001] dislocations in olivine are likely to exhibit the stable - non-planar - sessile configuration  
36 of Figure 2. This is consistent with the observation of long [001] screw dislocations. One can  
37 suppose that, under stress and in order to move, the core would need to transform into the  
38 metastable – planar - glissile configuration described by the Peierls model (Figure 3).  
39 Molecular dynamics modelling, perhaps along the lines reported by Marian et al. [49] for bcc  
40 iron, appears to be the most promising technique to probe this process. However, the  
41 important parameter is clearly the energy difference between the two cores, which is found to  
42 be large in the present case: 2.7 eV/Å. To give an idea, this energy difference is significantly  
43 larger than the highest Peierls energy barrier for glide of [100] Peierls dislocations (1.9 eV/Å),  
44 which requires a stress of almost 30 GPa to move [8]. Of course, core transformation  
45 processes will also be thermally activated. The energy difference for the sessile-glissile  
46 transitions must also be compared with the Peierls energy responsible for the friction opposed  
47 to glide of the glissile core. For [001](010) screw dislocations, the Peierls energy is 0.13 eV/Å  
48 [8], a value significantly lower than the threshold energy. The stress necessary to move the  
49 glissile dislocation is thus much lower than the threshold stress required to transform the core  
50  
51  
52  
53  
54  
55  
56  
57  
58  
59  
60

1  
2  
3 into the glissile configuration. This is characteristic of an unlocking mechanism as described  
4 by Couret and Caillard [50]. In that case, the metastable dislocations glide rapidly over a free-  
5 glide distance before falling back into a stable configuration (locking). The average mobility  
6 corresponding to this jerky motion is controlled by the unlocking and locking events. In situ  
7 deformation experiments in a transmission electron microscope would be highly desirable to  
8 check if this mechanism operates.  
9  
10  
11  
12  
13  
14

## 15 **5. Conclusion**

16  
17 The geometrical analysis of differential displacements within the core of a [001] screw  
18 dislocation suggests a 3D core as suggested by Durinck et al [8]. This observation is  
19 consistent with the microstructures observed in the TEM, where long screw segments are  
20 observed. Further modelling of the mobility of [001] dislocations is needed for a better  
21 understanding of the dislocation core under stress, of its ability to glide and possibly of the  
22 ability of the core to switch from a sessile (non-planar) configuration to a more mobile  
23 (planar) structure.  
24  
25  
26  
27  
28  
29  
30  
31

32 **Acknowledgements:** The authors warmly thank Dr. R. Groger for his help and for allowing  
33 use of the ddplot program. AMW acknowledges funding under the NERC Postdoctoral  
34 Research Fellowship scheme (NE/E012922/1).  
35  
36  
37  
38  
39  
40  
41  
42  
43  
44  
45  
46  
47  
48  
49  
50  
51  
52  
53  
54  
55  
56  
57  
58  
59  
60

## References

- [1] D.L. Kohlstedt and C. Goetze, *J. Geophys. Res.* 79 (1974) p.2045.
- [2] W.B. Durham, C. Goetze and B. Blake, *J. Geophys. Res.* 82 (1977) p.5755.
- [3] Y. Gueguen and M. Darot, *Philos. Mag. A* 45 (1982) p.419.
- [4] P. Cordier, in *Plastic deformation of minerals and rocks*, edited by S.-i. Karato and H.-R. Wenk (Mineral Society of America, Washington, DC, 2002), Vol. 51.
- [5] R. Von Mises, *Z. Angew. Math. Mech.* 8 (1928) p.161.
- [6] H. Couvy, D. Frost, F. Heidelbach, K. Nyilas, T. Ungár, S. Mackwell and P. Cordier, *Eur. J. Mineral.* 16 (2004) p.877.
- [7] J. Durinck, A. Legris and P. Cordier, *Am. Mineral.* 90 (2005) p.1072.
- [8] J. Durinck, P. Carrez and P. Cordier, *Eur. J. Mineral.* 19 (2007) p.631.
- [9] D. Mainprice, A. Tommasi, H. Couvy, P. Cordier and D.J. Frost, *Nature* 433 (2005) p.731.
- [10] P. Raterron, J.H. Chen, L. Li, D.J. Weidner and P. Cordier, *Am. Mineral.* 92 (2007) p.1436.
- [11] H.Y. Jung and S. Karato, *Science* 293 (2001) p.1460.
- [12] H. Jung, I. Katayama, Z. Jiang, I. Hiraga and S. Karato, *Tectonophysics* 421 (2006) p.1.
- [13] M.S. Duesbery and V. Vitek, *Acta Mater.* 46 (1998) p.1481.
- [14] G. Wang, A. Strachan, T. Cagin and W.A. Goddard III, *Phys. Rev. B* 68 (2003) p.224101.
- [15] J. Chaussidon, M. Fivel and D. Rodney, *Acta Mater.* 54 (2006) p.3407.
- [16] P. Phakey, G. Dollinger and J.M. Christie, *Geophys Monogr. Ser. - Flow and Fracture of Rocks* 13 (1972) p.117.
- [17] A.M. Walker, J.D. Gale, B. Slater and K. Wright, *Phys. Chem. Chem. Phys.* 7 (2005) p.3227.
- [18] A.M. Walker, J.D. Gale, B. Slater and K. Wright, *Phys. Chem. Chem. Phys.* 7 (2005) p.3235.
- [19] G. Schoeck, *Mater. Sci. Eng. A* 400-401 (2005) p.7.
- [20] G. Schoeck, *Acta Materialia* 54 (2006) p.4865.
- [21] C. Woodward, *Mater. Sci. Eng. A* 400-401 (2005) p.59.
- [22] C. Woodward, D.R. Trinkle, L.G.J. Hector and D.L. Olmsted, *Phys. Rev. Lett.* 100 (2008) art.n° 045507.

- 1  
2  
3 [23] R. Schroll, V. Vitek and P. Gumbsch, *Acta Mater.* 46 (1998) p.903.  
4  
5 [24] G. Schoeck, *Acta Mater.* 49 (2001) p.1179.  
6  
7 [25] C.R.A. Catlow, *Proc. R. Soc. Lond. Ser. A Math. Phys. Eng. Sci.* 353 (1977) p.533.  
8  
9 [26] M.J. Sanders, M. Leslie and C.R.A. Catlow, *Journal of the Chemical Society,*  
10 *Chemical Communications* (1984) p.1271.  
11  
12 [27] G.V. Lewis and C.R.A. Catlow, *J. Phys. C* 18 (1985) p.1149.  
13  
14 [28] G.D. Price, S.C. Parker and M. Leslie, *Phys. Chem. Minerals* 15 (1987) p.181.  
15  
16 [29] G.D. Price, S.C. Parker and M. Leslie, *Min. Mag.* 51 (1987) p.157.  
17  
18 [30] S.C. Parker and G.D. Price, *Adv. Solid-State Chem.* 1 (1989) p.295.  
19  
20 [31] G.W. Watson, P.M. Oliver and S.C. Parker, *Phys. Chem. Minerals* 25 (1997) p.70.  
21  
22 [32] N.H. de Leeuw, S.C. Parker, C.R.A. Catlow and G.D. Price, *Phys. Chem. Minerals* 27  
23 (2000) p.332.  
24  
25 [33] N.H. de Leeuw, S.C. Parker, C.R.A. Catlow and G.D. Price, *Am. Mineral.* 85 (2000)  
26 p.1143.  
27  
28 [34] K. Wright and C.R.A. Catlow, *Phys. Chem. Minerals* 20 (1994) p.515.  
29  
30 [35] J.A. Purton, N.L. Allan, J.D. Blundy and E.A. Wasserman, *Geochim. Cosmochim.*  
31 *Acta* 60 (1996) p.4977.  
32  
33 [36] J.A. Purton, N.L. Allan and J.D. Blundy, *Geochim. Cosmochim. Acta* 61 (1997)  
34 p.3927.  
35  
36 [37] A.M. Walker, S.M. Woodley, B. Slater and K. Wright, *Phys. Earth Planet. Int.* in press  
37 (2008).  
38  
39 [38] V.R. Saunders, C. Freyria-Fava, R. Dovesi and C. Roetti, *Comput. Phys. Comm.* 84  
40 (1994) p.156.  
41  
42 [39] J.D. Gale and A.L. Rohl, *Mol. Simulat.* 29 (2003) p.291.  
43  
44 [40] B. Joos, Q. Ren and M.S. Duesbery, *Phys. Rev. B* 50 (1994) p.5890.  
45  
46 [41] J.D. Eshelby, *Philos. Mag. A* 40 (1949) p.903.  
47  
48 [42] J.P. Hirth and J. Lothe, *Theory of dislocations*, John Wiley & Sons, Inc, New York,  
49 1982.  
50  
51 [43] J.F. Nye, *Physical properties of crystals*, Oxford University Press, Oxford, UK, 1957.  
52  
53 [44] J.W. Steeds, *Introduction to Anisotropic Elasticity Theory of Dislocations*, Clarendon  
54 Press, Oxford, UK, 1973.  
55  
56 [45] V. Vitek, R.C. Perrin and D.K. Bowen, *Philos. Mag. A* 21 (1970) p.1049.  
57  
58 [46] A.M. Walker, K. Wright and B. Slater, *Phys. Chem. Minerals* 30 (2003) p.536.  
59  
60 [47] L. Trépiéd and J.C. Doukhan, *Phys. Stat. Sol (a)* 49 (1978) p.713.

- 1  
2  
3 [48] V. Vitek, Phys. Stat. Sol (b) 18 (1966) p.687.  
4  
5 [49] J. Marian, W. Cai and V.V. Bulatov, Nature Materials 3 (2004) p.158.  
6  
7 [50] A. Couret and D. Caillard, Philos. Mag. A 59 (1989) p.783.  
8  
9  
10  
11  
12  
13  
14  
15  
16  
17  
18  
19  
20  
21  
22  
23  
24  
25  
26  
27  
28  
29  
30  
31  
32  
33  
34  
35  
36  
37  
38  
39  
40  
41  
42  
43  
44  
45  
46  
47  
48  
49  
50  
51  
52  
53  
54  
55  
56  
57  
58  
59  
60

For Peer Review Only

| Charges (units of electronic charge) |                             |                         | Core – shell spring constant ( $\text{eV}\text{\AA}^{-2}$ ) |
|--------------------------------------|-----------------------------|-------------------------|---|
| Ion                                  | Core                        | Shell                   |   |
| Mg                                   | 2.0                         |                         |   |
| Si                                   | 4.0                         |                         |   |
| O                                    | 0.84819                     | -2.84819                | 74.92038  |
| Buckingham potential                 | $A$ (eV)                    | $\rho$ ( $\text{\AA}$ ) | $C$ ( $\text{eV}\text{\AA}^{-6}$ )                          |
| Si – O                               | 1283.90734                  | 0.32052                 | 10.66158  |
| Mg – O                               | 1428.5                      | 0.29453                 | 0.0   |
| O – O                                | 22764.0                     | 0.1490                  | 27.88   |
| Harmonic three-body                  | $k$ ( $\text{eVrad}^{-2}$ ) | $\theta_0$ (degrees)    |   |
| O – Si – O                           | 2.09724                     | 109.47                  |   |

Table 1: Parameters of the potential model. Pair potentials are truncated beyond 10  $\text{\AA}$  and three body terms only act between bonded  $\text{SiO}_4$  groups.

|       | DFT   |                                     |                                  | Parameterised potentials                              |                                     |                                  |
|-------|---|-------------------------------------|----------------------------------|---|-------------------------------------|----------------------------------|
|       | $\gamma^{\text{max}}$<br>( $\text{eV}/\text{\AA}^2$ ) | SFE<br>( $\text{eV}/\text{\AA}^2$ ) | $\gamma^{\text{max}}/\text{SFE}$ | $\gamma^{\text{max}}$<br>( $\text{eV}/\text{\AA}^2$ ) | SFE<br>( $\text{eV}/\text{\AA}^2$ ) | $\gamma^{\text{max}}/\text{SFE}$ |
| {110} | 0.077   | 0.024                               | 3.2                              | 0.115   | 0.042                               | 2.7                              |
| (100) | 0.037   | 0.019                               | 1.9                              | 0.048   | 0.043                               | 1.1                              |
| (010) | 0.128   | -                                   | -                                | 0.150   | -                                   | -                                |

Table 2: Principal parameters,  $\gamma^{\text{max}}$  and stacking fault energy (SFE), of GSF calculations depending on the calculation method.

1  
2  
3  
4  
5  
6  
7  
8  
9  
10  
11  
12  
13  
14  
15  
16  
17  
18  
19  
20  
21  
22  
23  
24  
25  
26  
27  
28  
29  
30  
31  
32  
33  
34  
35  
36  
37  
38  
39  
40  
41  
42  
43  
44  
45  
46  
47  
48  
49  
50  
51  
52  
53  
54  
55  
56  
57  
58  
59  
60

## Figures

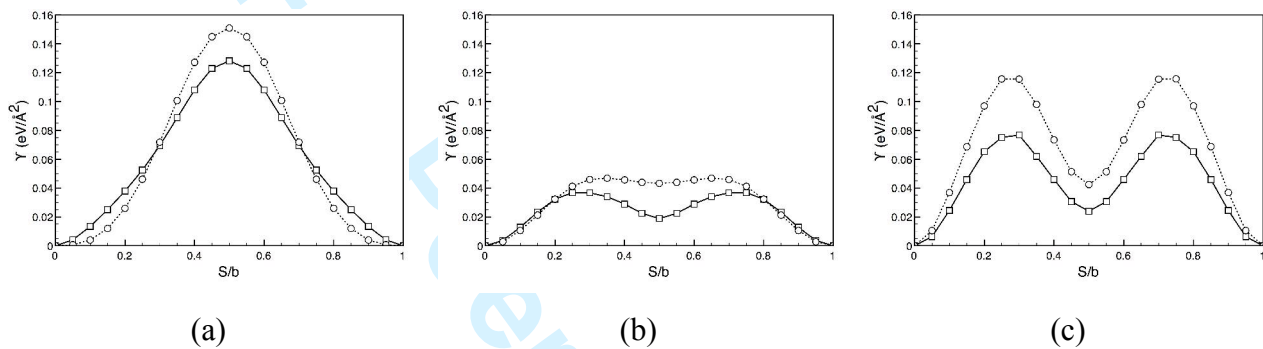


**Figure 1:** Generalised Stacking Faults (GSF) corresponding to a [001] shear in (010), (100) and (110). The GSF are given for both VASP (squares) and GULP (circles) calculations as a function of  $S/b$  where  $S$  is the shear amount and  $b$  the modulus of [001].

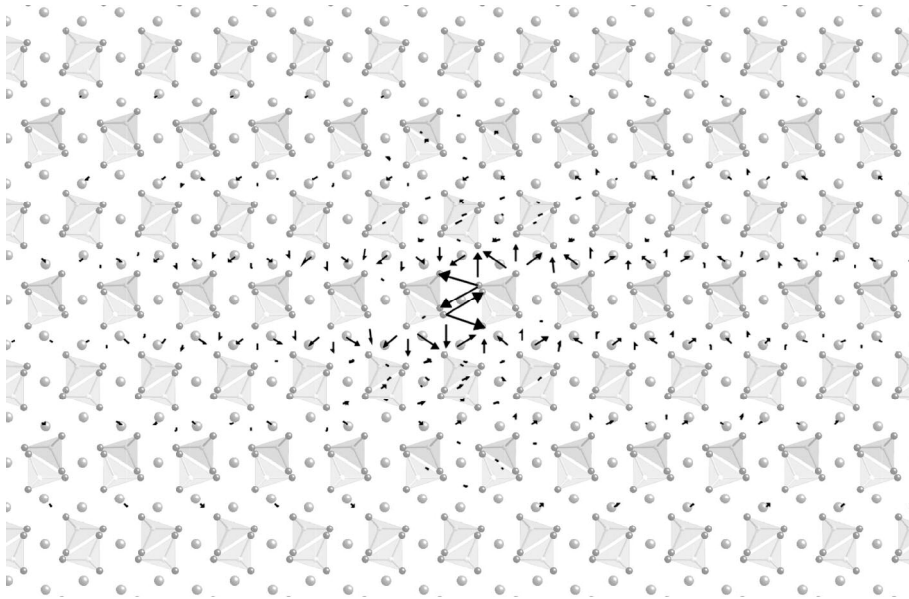


**Figure 2:** Differential displacement map for the [001] screw dislocation calculated by direct simulation by Walker et al. [18]. The dislocation is viewed end on (i.e. along the [001] direction)

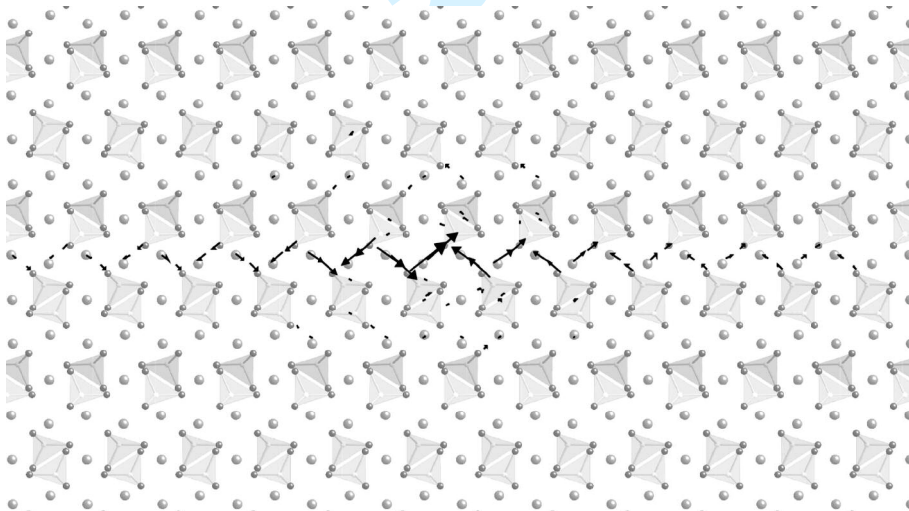
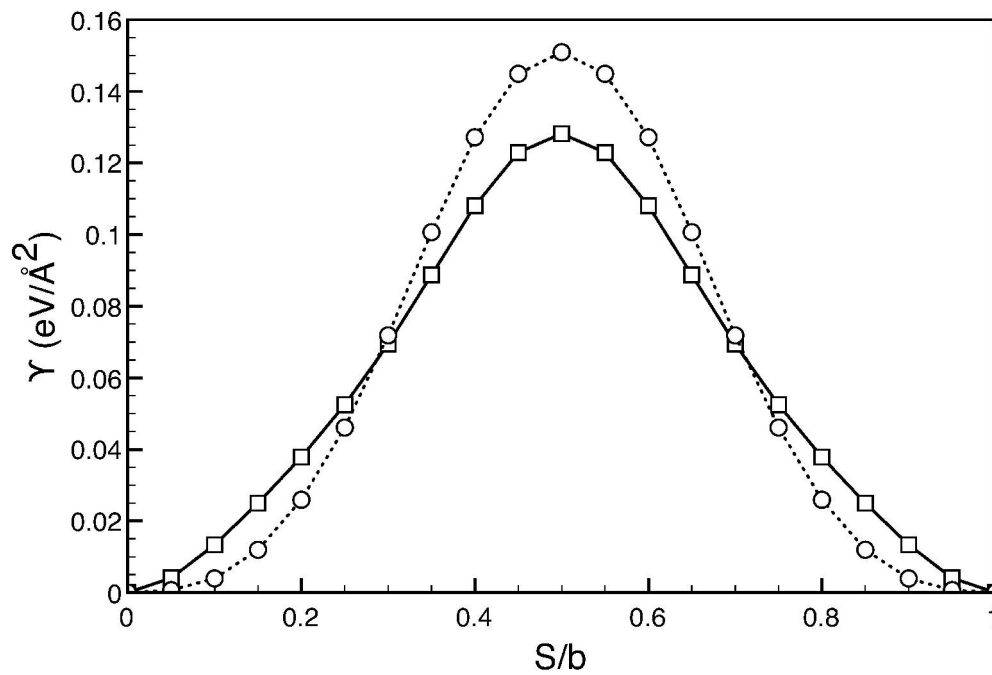
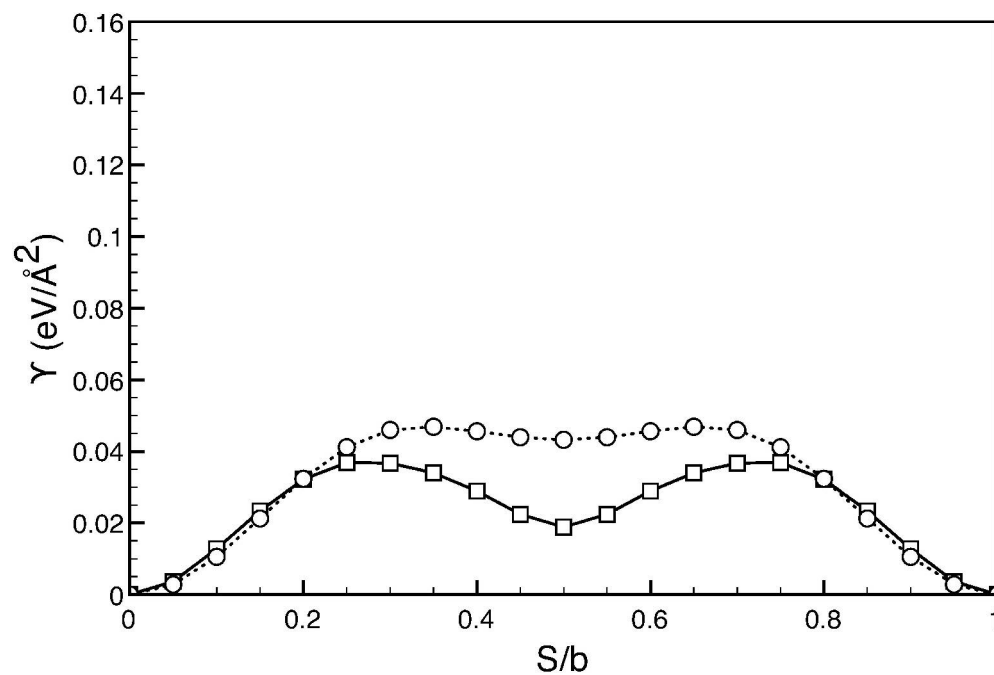


**Figure 3:** Differential displacement map for the Peierls [001](010) screw dislocation

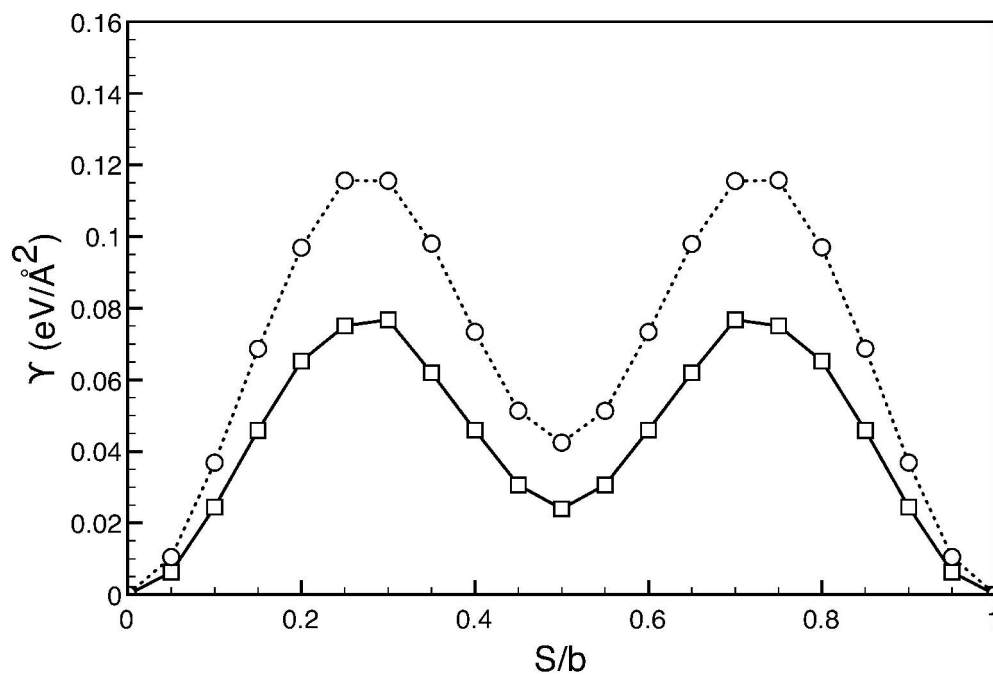


239x169mm (600 x 600 DPI)

view Only



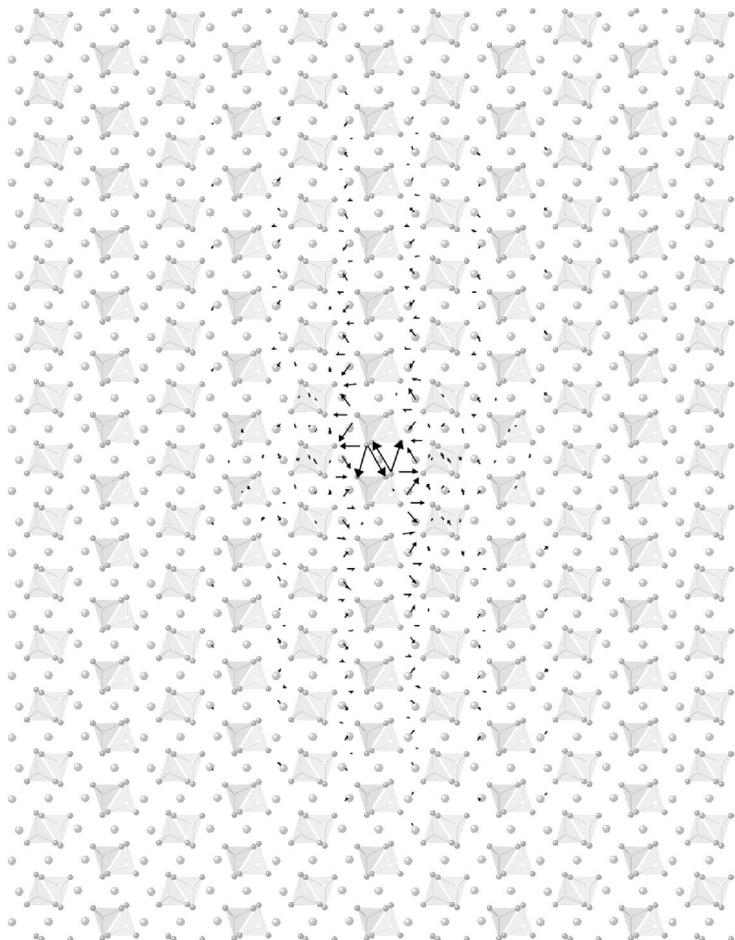
239x169mm (600 x 600 DPI)



239x169mm (600 x 600 DPI)

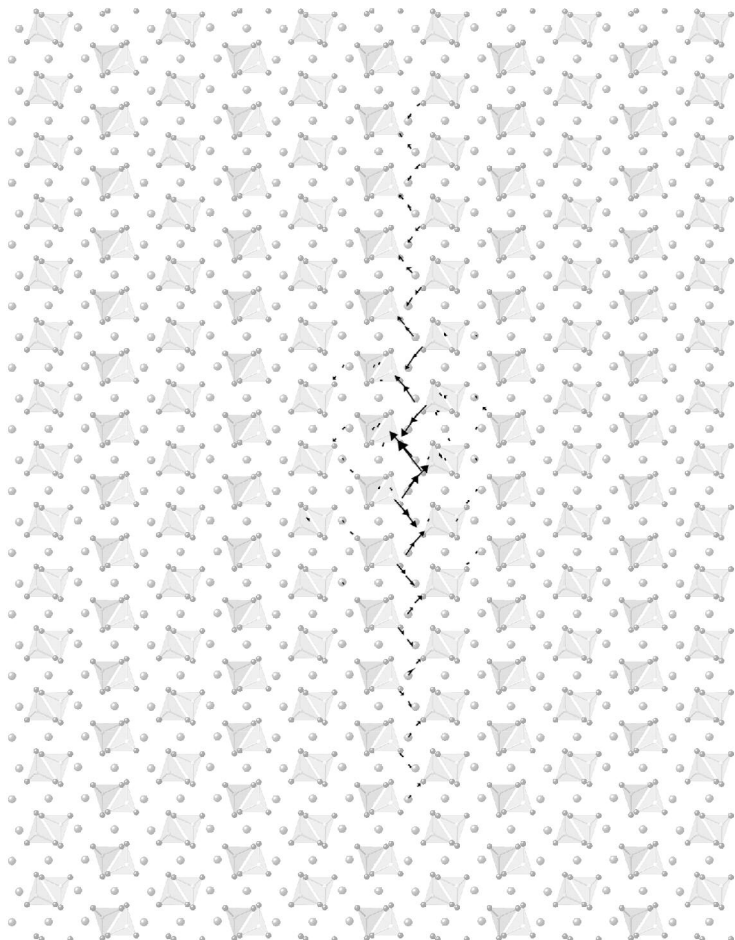
View Only

1  
2  
3  
4  
5  
6  
7  
8  
9  
10  
11  
12  
13  
14  
15  
16  
17  
18  
19  
20  
21  
22  
23  
24  
25  
26  
27  
28  
29  
30  
31  
32  
33  
34  
35  
36  
37  
38  
39  
40  
41  
42  
43  
44  
45  
46  
47  
48  
49  
50  
51  
52  
53  
54  
55  
56  
57  
58  
59  
60



209x297mm (600 x 600 DPI)

1  
2  
3  
4  
5  
6  
7  
8  
9  
10  
11  
12  
13  
14  
15  
16  
17  
18  
19  
20  
21  
22  
23  
24  
25  
26  
27  
28  
29  
30  
31  
32  
33  
34  
35  
36  
37  
38  
39  
40  
41  
42  
43  
44  
45  
46  
47  
48  
49  
50  
51  
52  
53  
54  
55  
56  
57  
58  
59  
60



209x297mm (600 x 600 DPI)